Quantitative Phosphoproteomics of Early Elicitor Signaling in *Arabidopsis**[S]

Joris J. Benschop‡§¶, Shabaz Mohammed§‖, Martina O'Flaherty‖, Albert J. R. Heck‖, Monique Slijper‖, and Frank L. H. Menke‡ ‡‡**

Perception of general elicitors by plant cells initiates signal transduction cascades that are regulated by protein phosphorylation. The earliest signaling events occur within minutes and include ion fluxes across the plasma membrane, activation of MAPKs, and the formation of reactive oxygen species. The phosphorylation events that regulate these signaling cascades are largely unknown. Here we present a mass spectrometry-based quantitative phosphoproteomics approach that identified differentially phosphorylated sites in signaling and response proteins from *Arabidopsis* cells treated with either flg22 or xylanase. Our approach was sensitive enough to quantitate phosphorylation on low abundance signaling proteins such as calcium-dependent protein kinases and receptor-like kinase family members. With this approach we identified one or more differentially phosphorylated sites in 76 membrane-associated proteins including a number of defense-related proteins. Our data on phosphorylation indicate a high degree of complexity at the level of post-translational modification as exemplified by the complex modification patterns of respiratory burst oxidase protein D. Furthermore the data also suggest that protein translocation and vesicle traffic are important aspects of early signaling and defense in response to general elicitors. Our study presents the largest quantitative *Arabidopsis* phosphoproteomics data set to date and provides a new resource that can be used to gain novel insight into plant defense signal transduction and early defense response. ***Molecular & Cellular Proteomics 6:1198–1214, 2007.***

Plants have developed various elaborate mechanisms to ward off pathogen attack. Whereas some of these defense mechanisms are preformed and provide physical and chemical barriers to hinder pathogen infection, others are induced only upon pathogen perception. These different layers of defense include basal defense and resistance (R)[1]-gene-mediated defenses. Plants use R-gene products to recognize the presence or activity of specific pathogen avirulence gene products produced by specific races of microbial pathogens in a so-called gene-for-gene interaction. A specific match between an avirulence gene product and the corresponding R-gene product leads to hypersensitive response and activation of defense responses. In addition to R-gene-mediated defense plants rely on recognition of general elicitors, also called pathogen-associated molecular patterns, to detect potential pathogens and to activate basal defense (1). These general elicitors are structural components of microbes that are recognized by plants through plasma membrane-localized receptors. The general elicitor flagellin is recognized in *Arabidopsis* through a conserved 22-amino acid sequence (flg22). Recognition involves the receptor-like kinase FLS2 and activates a downstream response that includes the production of reactive oxygen species, ethylene biosynthesis, activation of a MAPK cascade, and activation of defense gene expression (2–4). Furthermore perception of flg22, as well as other general elicitors, by *Arabidopsis* enhances disease resistance against bacterial pathogens (5). Perception of both avirulence gene products and general elicitors activates signal transduction cascades and early defense responses to prevent the ingression of the pathogen into host tissue. A recent study established that flg22-induced response in *Arabidopsis* and Avr9-induced response in tobacco show a substantial amount of overlap (6). Furthermore Tao *et al.* (7) have shown that the transcriptional reprogramming in response to compatible and incompatible interactions is very similar and that the difference in outcome likely depends on the quantitative nature of the local defense response (7).

The signal transduction pathways activated by general elicitors and *Avr* gene products are not well characterized. Thus far, research on plant defense signaling has focused mainly on the genetic dissection of the signal transduction pathways. Although the analysis of mutants with altered defense re-

From the ‡Molecular Genetics, Utrecht University, Padualaan 8, 3584CH Utrecht, The Netherlands and ‖Department of Biomolecular Mass Spectrometry, Bijvoet Center for Biomolecular Research and Utrecht Institute for Pharmaceutical Sciences, Utrecht University, Sorbonnelaan 16, 3584CA Utrecht, The Netherlands

Received, November 13, 2006, and in revised form, February 9, 2007

Published, MCP Papers in Press, February 21, 2007, DOI 10.1074/mcp.M600429-MCP200

[1] The abbreviations used are: R, resistance; BIK1, Botrytis-Induced Kinase1; CDPK, calcium-dependent protein kinase; flg22, conserved 22-amino acid sequence of flagellin of pathogenic *Pseudomonas*; LTQ, linear ion trap; MAP, mitogen-activated protein; MAPK, mitogen-activated protein kinase; PM, plasma membrane; RLK, receptor-like kinase; ROI, reactive oxygen intermediate; SCX, strong cation exchange chromatography; SILAC, stable isotope labeling by amino acids in cell culture; SNARE, soluble *N*-ethylmaleimide-sensitive factor attachment protein receptor; TiO_2, titanium oxide; ABC, ATP-binding cassette; RBOHD, respiratory burst oxidase protein D.

sponses has yielded a variety of putative defense signaling components, the molecular mechanisms these signaling components affect remain elusive. However, reverse and forward genetic approaches have pointed to an important role for protein phosphorylation in defense signaling. Mutations in the Pto serine/threonine kinase in tomato (8) and Xa21 leucine-rich repeat kinase in rice (9) compromise the plant's resistance to race-specific pathogens, whereas mutations in receptor-like kinase FLS2 in *Arabidopsis* enhances susceptibility to *Pseudomonas syringae* pv. *tomato* DC3000 (5). Silencing of tobacco MAPK kinase kinase NPK1 and *Arabidopsis* MAPK MPK6 also compromises disease resistance (10, 11). The perception of general elicitors and downstream signal transduction has been studied intensively with biochemical and pharmacological approaches and more recently with transient expression approaches in protoplasts (2, 12–16). This has led to the identification of several early signaling events, including ion fluxes across the plasma membrane, extracellular alkalinization, transient increases in cytosolic calcium concentration, protein phosphorylation and dephosphorylation through activation of MAPK and calcium-dependent protein kinases (CDPKs), and the production of extracellular reactive oxygen species through PM-localized NADPH oxidase and apoplastic peroxidase and biosynthesis of ethylene and jasmonic acid (13, 16, 17). Eventually both receptor-mediated perception of general elicitors and R-gene-mediated detection of avirulence proteins lead to the activation of transcriptional cascades and the expression of defense responses.

By definition, the proteins that make up the signal transduction pathway are present in the cell prior to the perception of the elicitor. They are activated by post-translational modifications, conformational changes, and/or changes in complex formation. The most widely recognized post-translational modification involved in signal transduction is protein phosphorylation. Although protein kinases and phosphatase have been identified with a role in defense signaling and resistance, their exact role and their substrates have remained elusive in plants. General elicitor signaling is thought to be initiated through interaction of the elicitor with a plasma membrane-localized receptor. Immediate early signaling and responses are likely mediated through plasma membrane-associated proteins. Recent work showed that many membrane-associated proteins have one or more phosphorylation sites (18). Furthermore phosphorylated proteins have been detected in the extracellular matrix of *Arabidopsis* suspension cultured cells in response to fungal elicitor (15). However, the functionality of only a very few of these is currently understood. The large scale identification of phosphorylation sites as well as the kinetics and stoichiometry of the phosphorylation status will help unravel the immediate early signal transduction cascades and defense response in response to general elicitors.

Detection of changes in protein phosphorylation was traditionally performed by labeling cells with radioactive phosphate followed by two-dimensional gel separation of labeled proteins and mass spectrometric analysis (19). Recent advances in LC-MS/MS have made it possible to directly analyze highly complex protein mixtures. Unfortunately traditional LC-MS/MS experiments generally yield few phosphorylated peptides. Despite the fact that a high percentage of cellular proteins are thought to be phosphorylated at any given time (20), this phosphorylated form is generally low in abundance. Furthermore the addition of a phosphate group often results in a reduction in ionization efficiency in MS (21). Recent advances in selective purification of phosphopeptides have made it possible to overcome these limitations and identify phosphorylation sites in large numbers of proteins (18, 22, 23). Although these qualitative approaches are highly informative in themselves, the identification of phosphorylation events relevant to a specific signaling pathway requires quantitative rather than qualitative measurements. Quantitative phosphoproteomics approaches based on stable isotope labeling by amino acids in cell culture (SILAC) have been successfully applied in studies with cultured human cells and in yeast (24–26) and could in principle also be used in studies with plant cell cultures. An alternative approach, called iTRAQ (isobaric tagging for relative and absolute quantitation), has been described recently in several quantitative phosphoproteomics studies (27, 28) and is based on the labeling of the N termini and lysine residues of extracted (phospho-)peptides with isobaric tags to allow quantitation. Here we report an alternative quantitative phosphoproteomics approach, based on $^{14}N/^{15}N$ metabolic labeling, that is specifically suited for cultured plant cells.

We set up this quantitative phosphoproteomics approach to identify the early signaling and response proteins modulated upon perception of general elicitors by *Arabidopsis* cells. We used a $^{14}N/^{15}N$ metabolic labeling strategy that allowed us to directly compare phosphorylation levels of proteins of mock-treated and elicitor-treated cells with mass spectrometry. Changes in phosphorylation of membrane-associated proteins were analyzed for cells treated with the flagellin peptide flg22 and fungal elicitor xylanase. Quantitative changes in phosphorylation were compared between the two resulting data sets so that proteins phosphorylated in response to both elicitors could be identified. Our data identify quantitative changes in phosphorylation of novel membrane-associated proteins as well as established defense-related proteins. Additionally our data also point to a role for protein translocation and vesicle transport during early elicitor signaling and response.

EXPERIMENTAL PROCEDURES

Materials

Poros R3 was obtained from Applied Biosystems (Nieuwerkerk a/d IJssel, The Netherlands). $K^{15}NO_3$ and $(^{15}NH_4)_2SO_4$ were from Spectra Stable Isotopes (Columbia, MD). Flagellin peptide flg22 was synthesized by Sigma Genosys. Modified trypsin was from Roche Applied

Science. GeLoader tips came from Eppendorf (Eppendorf, Germany). The Empore C_8 disk was from 3M (Neuss, Germany). Syringes and needles were from SGE (Victoria, Australia). All other chemicals were obtained from Sigma-Aldrich.

Growth of Cells

Suspension cells of *Arabidopsis thaliana* accession Col-0 (29) were cultured on Gamborg B5 medium (30 g/liter sucrose, 1 mM naphthaleneacetic acid, 1.0 mM $(NH_4)_2SO_4$, 25 mM KNO_3, 1.1 mM $NaH_2PO_4{\cdot}H_2O$, 1.0 mM $CaCl_2{\cdot}2H_2O$, 1.0 mM $MgSO_4{\cdot}7H_2O$, 100 μM FeNaEDTA, 60 μM $MnSO_4{\cdot}H_2O$, 50 μM H_3BO_3, 7.0 μM $ZnSO_4$, 1.0 μM Na_2MoO_4, 4.5 μM KI, 0.10 μM $CoCl_2$, 0.10 μM $CuSO_4$, and 112 mg/ml vitamin mixture (G0415, Duchefa, Haarlem, The Netherlands)) in 50-ml cultures in 250-ml flasks with shaking at 150 rpm. Growth conditions were 8 h of light of 70 μM m^{-2} s^{-1} photosynthetic photon flux density at 25 °C. Cells were subcultured (4 ml in 50 ml) every 7 days. Experiments were performed 5 days after subculturing.

Elicitor Treatment and Isolation of Membrane Proteins

Elicitor Treatment and Harvest—Cultures were grown for at least 4 subculture periods of 7 days on either ^{14}N- or ^{15}N-medium prior to elicitor induction. Four-day-old cultures were treated for exactly 10 min with 100 μg/ml xylanase or 1 μM flg22. For the first biological replicate, three separately treated (^{14}N) cultures and three mock-treated (^{15}N) cultures were pooled, harvested by filtration, washed with ice-cold 20 mM KNO_3, and resuspended in homogenization buffer (100 mM HEPES, 330 mM sucrose, 10 mM Na_2EDTA, 10 mM EGTA, 50 mM sodium pyrophosphate, 25 mM NaF, 1 mM $NaMoO_4$, 1 mM $MgCl_2$, 5 mM DTT, 1 mM ascorbic acid, 1 mM Na_3VO_4, 5 g/liter polyvinylpolypyrrolidone, 1 μg/ml leupeptin, 1 μg/ml pepstatin A, and 1 μg/ml aprotinin) at a ratio of 2 ml/g of cells. This was done seven times for a total of 21 cultures of each treatment type per experiment, and the homogenates were pooled before PM isolation. In the second biological replicate ^{15}N-grown cultures were elicitor-treated, and ^{14}N-grown cultures were mock-treated. Both elicitor treatments and both biological replicas were done independently with a 7-day period between each treatment and each replica.

Isolation of Plasma Membranes—Cells were broken in a 60-ml Potter-Elvehjem homogenizer on ice (8 min at 1000 rpm). The homogenate was centrifuged for 10 min at 10,000 × *g* (Sorvall SW34 rotor). The supernatant was centrifuged for 1 h at 100,000 × *g* (Beckman SW28 rotor). The pellet was resuspended in a buffer containing 330 mM sucrose, 5 mM KPO_4, pH 7.8, and 5 mM KCl and subjected to aqueous two-phase partitioning (30) using 6.4% (w/w) each of dextran T500 and polyethylene glycol 3350 with 5 mM KCl and 5 mM KPO_4, pH 7.8. The U3 phase was diluted 2-fold in buffer containing 330 mM sucrose and 5 mM KPO_4, pH 7.8. Plasma membranes were pelleted at 100,000 × *g* for 1 h (Beckman SW28 rotor), resuspended to a concentration of 10 μg/μl, frozen in liquid nitrogen, and stored at −80 °C.

Flipping, Alkylation, and Digestion—Plasma membranes containing 4 mg of protein (50% of the total isolate) were mixed with a solution containing 2% (w/v) Brij58 in 330 mM sucrose and 5 mM KPO_4 with inhibitors (1 mM $NaVO_3$, 1 mM $NaMoO_4$, 25 mM NaF, 1 μg/μl leupeptin, 1 μg/μl aprotinin, 1 μg/μl pepstatin, and 1 mM PMSF) to a detergent:protein ratio of 3:1 (w/w). After centrifugation (200,000 × *g* for 1 h) the pellet was resuspended in 200 mM KCl and 30 mM DTT with inhibitors and incubated for 2 h at room temperature. This was centrifuged again, and the pellet was resuspended in 50 mM iodoacetamide in 50 mM NH_4HCO_3 and kept at room temperature for 30 min in darkness. One more wash with 50 mM NH_4HCO_3 was performed, and the final pellet was resuspended in 250 μl of 50 mM NH_4HCO_3. Proteins were digested with trypsin (ratio, 1:50) overnight at 37 °C. The solution was acidified with formic acid (5% end concentration) and centrifuged as above. The supernatant was then brought to a final volume of 40 μl under reduced pressure.

Selective Enrichment of Phosphopeptides

Strong Cation Exchange Chromatography—Strong cation exchange chromatography (SCX) was performed according to Gruhler *et al.* (26) on an ammonium formate gradient. Prior to SCX the digested peptides were desalted on a 15-μl POROS R3 reverse phase column made in a constricted GeLoader tip (31). Peptides were eluted with 40 μl of 50% acetonitrile and diluted to yield 100 μl with SCX buffer A. Peptides were separated on a 1-ml Resource S column (GE Healthcare) on an ÁKTA purifier (GE Healthcare). 16 fractions were collected, reduced in volume to 20 μl, and frozen at −20 °C.

Titanium Oxide Enrichment—Titanium oxide (GL Sciences Inc., Tokyo, Japan) columns were prepared by placing a small plug, stamped out of a 3M Empore C_8 disk using a 0.3-mm-inner diameter flat tip needle fitted on a 1-ml glass syringe and brought to position using a 0.15-mm-outer diameter wire just above the constricted end of a GeLoader tip. The column material was then packed to a bedding volume of 1 μl (±2 cm) and washed with washing buffer (80% acetonitrile in 0.1% TFA). Samples were loaded on a 3-μl reverse phase column as described above and eluted with 15 μl of titanium oxide (TiO_2) loading buffer (80% acetonitrile, 0.1% TFA, and 300 mg/ml dihydroxybenzoic acid). This eluate was loaded slowly onto the TiO_2 column and washed with 6 μl of loading buffer and 6 μl of washing buffer. Phosphopeptides were eluted with 20 μl of 1% ammonia. The eluate was mixed with 20 μl of 10% formic acid and frozen at −20 °C prior to MS analysis.

Mass Spectrometry

Nanoscale HPLC-MS/MS experiments were performed on an Agilent 1100 nanoflow system (Agilent Technologies) connected to a 7-tesla Finnigan LTQ-FT mass spectrometer (Thermo Electron, Bremen, Germany) equipped with a nanoelectrospray ion source. Loading was accomplished by using a flow rate of 5 μl/min onto a homemade 2-cm fused silica precolumn (100-μm inner diameter, 375-μm outer diameter, Resprosil C18-AQ, 3 μm (Maisch, Ammerbuch, Germany)) using an autosampler. Sequential elution of peptides was accomplished using a linear gradient from Solution A (0.6% acetic acid) to 50% Solution B (80% acetonitrile and 0.5% acetic acid) in 40 min over the precolumn in line with a homemade 20–25-cm resolving column (50-μm inner diameter, 375-μm outer diameter, Resprosil C18-AQ, 3 μm (Maisch)).

The mass spectrometer was operated in the data-dependent mode to automatically switch between MS, MS/MS, and neutral loss-dependent MS/MS/MS (MS^3) acquisition. Survey full-scan MS spectra (from *m/z* 300 to 1500) were acquired in the FT-ICR mass spectrometer with resolution $R = 25{,}000$ at *m/z* 400 (after accumulation to a target value of 5,000,000 in the linear ion trap). The three most intense ions were sequentially isolated for accurate mass measurements by a FT-ICR "single ion monitoring scan," which consisted of a 15-Da mass range, resolution $R = 50{,}000$, and target accumulation value of 80,000. These were then simultaneously fragmented in the linear ion trap using collisionally induced dissociation at a target value of 10,000.

The data-dependent neutral loss algorithm in the Xcalibur software was enabled for each MS/MS spectrum. Data-dependent settings were chosen to trigger a MS^3 scan when a neutral loss corresponding to 98, 49, or 32.7 Th was detected among the five most intense fragment ions. Former target ions selected for MS/MS were dynamically excluded for 30 s. Total cycle time was approximately 3 s.

Each sample was also subjected to a "regular" LC-MS/MS analy-

sis. Survey full-scan MS spectra (from *m/z* 300 to 1500) were acquired in the FT-ICR mass spectrometer with resolution $R = 100{,}000$ at *m/z* 400 (after accumulation to a target value of 2,000,000 in the linear ion trap). The two most intense ions were fragmented in the linear ion trap using collisionally induced dissociation at a target value of 10,000.

Data Analysis

All MS/MS spectra files from each LC run were centroided and merged to a single file using Bioworks 3.2 (Thermo Electron), which was searched using the Mascot search engine (version 2.1.0, Matrix Science) against the publicly available *Arabidopsis* database (The *Arabidopsis* Information Resource (TAIR); August 2005; file name, ATH1_pep_cm_20040228; containing 29,161 non-redundant proteins) with carbamidomethylcysteine as a fixed modification. Oxidized methionine and phosphorylation (serine, threonine, and tyrosine) were searched as variable modifications. Searches were done with tryptic specificity allowing two miscleavages and an initial tolerance on mass measurement of 20 ppm in MS mode and 0.9 Da for MS/MS ions. To perform relative quantification the same files were rerun under the same search criteria but with the database consisting of proteins with masses incorporating ^{15}N. A score cutoff of 50 was used (stated if otherwise) that corresponds to an expect value in the region of 0.001 to create a data set with high confidence. All MS^2 Mascot data is available as a scaffold file (Proteome Software, Portland, OR) upon request. An appropriate reader is also available. Some peptides were observed that could be derived from multiple proteins (Supplemental Table VII). These peptides were assigned to the protein for which we identified the highest number of peptides with a Mascot score of 50 or higher.

Relative quantification ratios of the identified phosphopeptides were derived by MSQuant. Briefly peptide ratios between the monoisotopic peaks of "normal" and "heavy" forms of the phosphopeptide were calculated and averaged over consecutive MS cycles for the duration of their respective LC-MS peaks in the total ion chromatogram using both FT survey and FT single ion monitoring scans. All identified phosphopeptides that were differentially phosphorylated and that could be confirmed in both biological replicates of either the flg22 data set or the xylanase data set were manually validated (spectra are provided as supplemental data). Localization of phosphorylated residues within the individual peptide sequences were manually assigned using the software packages MSQuant (which is open-source software (70)) and Xcalibur (Thermo, San Jose, CA). All phosphopeptides that were not differentially phosphorylated or could only be observed in one biological replica are provided as supplemental data. Only those phosphopeptides were included that have a Mascot score of at least 50 (Supplemental Tables II and III).

All data were normalized to the mean of all ratios of unmodified peptides within each biological replicate. Subsequently data for each peptide from both biological replicas were averaged.

RESULTS AND DISCUSSION

Induction, Extraction, and Purification of Phosphopeptides

Perception of general elicitors occurs at the external side of the plasma membrane and sets in motion a signal transduction cascade. We used flagellin peptide flg22 and xylanase as general elicitors to activate early signal transduction in *Arabidopsis* suspension cultured cells. Perception of flg22 or xylanase activates MAP kinases in *Arabidopsis* suspension cultured cells within minutes; MAP kinase activity peaks within 5–10 min and diminishes after 30 min (Fig. 1). Based on these activation kinetics we chose 10-min incubation with flg22 or xylanase for our further experiments.

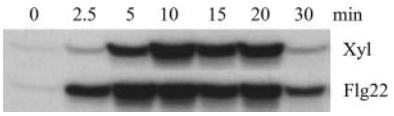

FIG. 1. **Elicitor-induced MAP kinase activation in *Arabidopsis* cells.** *Arabidopsis* cells were incubated for the indicated amount of time in minutes with either 1 μM flg22 or 100 μg/ml xylanase (*Xyl*). MAP kinase activity in protein extracts from treated cells was analyzed by in-gel kinase assay.

The initial signaling events are likely to occur at the cytosolic face of the plasma membrane so we set out to identify signal transduction proteins associated with the plasma membrane. This strategy resulted in a considerable reduction in complexity of the proteome and allowed us to focus on the earliest signaling events. We used aqueous two-phase partitioning (32–34) to obtain purified plasma membrane vesicles. To verify the efficiency of the method, we analyzed the crude microsomal samples and purified PM samples by Western blot probed with antibodies specific for marker proteins of different cellular compartments (Fig. 2*a*). This showed a significant enrichment for PM proteins, whereas mitochondrial and vacuolar proteins were almost entirely absent from the PM sample (Fig. 2*a*).

From these PM vesicles we prepared a tryptic digest of the cytosolic domain using the vesicle shaving method (34).To obtain further reduction in complexity of the sample, trypsin-digested peptides were fractioned using SCX under acidic conditions (Fig. 2*c*), which separates phosphopeptides from the majority of the non-phosphopeptides due to differences in solution state charge (35). Subsequently each fraction was separately enriched for phosphopeptides using TiO_2 affinity chromatography (23) in the presence of high concentrations of dihydroxybenzoic acid (36). Fig. 2*d* shows that early SCX fractions consisted almost entirely of singly phosphorylated peptides after TiO_2 enrichment, whereas later fractions also contained a significant number of multiple phosphorylated as well non-phosphorylated peptides. Of the 1168 detected phosphopeptides we identified mostly phosphorylated Ser and Thr residues (Ser(P), 979 (83%); Thr(P), 189 (17%); Supplemental Table V) and only a few (11) phosphorylated Tyr residues (data not shown). A more detailed description of the analytical performance of the enrichment strategy and the physiochemical properties of all identified peptides is provided in the supplemental data.

MS Analysis

The comparative analysis of protein sample by MS is hampered by the fact that sample preparation, purification strategies, and MS analysis results in semiquantitative data at best. To overcome these limitations, two different samples can be "tagged" with different mass labels and analyzed together. This allows for a pairwise comparison of signal

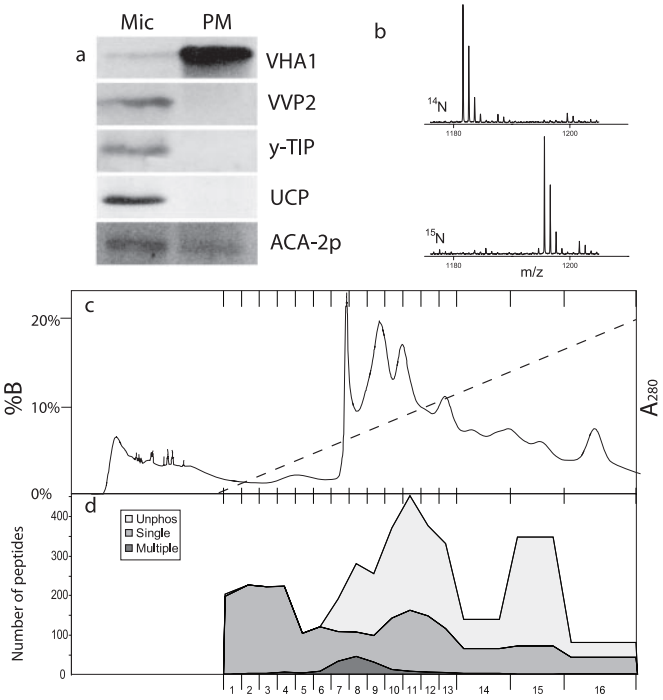

FIG. 2. **Enrichment and quantitative labeling of plasma membrane phosphopeptides.** *a*, Western blot of total microsomal membranes (*Mic*) and purified PM with antibodies against PM ATPase VHA1, vacuolar VVP2, and γ-tonoplast intrinsic protein (γ-TIP), mitochondrial uncoupling protein (UCP), and endoplasmic reticulum-located ACA-2p. Total protein content was similar in all lanes. *b*, MALDI spectrum of a peptide isolated from a complete lysate of cells grown on ^{14}N- or ^{15}N-medium. The MALDI spectra correlate to the peptide GVTAFGFDLVR from the protein 5-methyltetrahydropteroyltriglutamate-homocysteine methyltransferase (At5g17920). The sample used in the *top spectrum* originates from a ^{14}N-labeled sample (peak *m/z* value ^{14}N: 1181.620), whereas the sample used for the *bottom spectrum* originates from a ^{15}N-labeled sample (peak *m/z* value ^{15}N: 1195.612). *c*, tryptic peptides were subjected to SCX, and a chromatogram is shown depicting UV absorbance at 280 nm. The gradient of SCX solvent B is indicated with a *dashed line*. Fractions collected and analyzed are as shown in *d*. *d*, the number of phosphorylated and unphosphorylated (*Unphos*) peptides identified in each fraction collected from SCX (fractions 1–16 were analyzed by LC-MS).

intensities for each peptide in the sample similar to the use of different fluorescent dyes during competitive hybridization in microarray experiments. As extraction efficiencies can be different between samples, optimal quantitative accuracy is achieved when the two samples are tagged and combined prior to the extraction. This can be achieved by growing cells on medium containing specific ^{15}N-amino acids or on a basal salt medium containing ^{15}N as a sole nitrogen source, so-called metabolic labeling (37). SILAC, a metabolic labeling method that uses ^{15}N-labeled lysine and arginine (38), is an elegant method to achieve *in vivo* tagged proteins where the mass shift between the two isotopic forms of the peptide is independent of their size or sequence; this strongly simplifies the quantitation procedure. However, due to autonomous production of these amino acids in plant cells only partial incorporation can be achieved in *Arabidopsis* (39). In contrast, Krijgsveld *et al.* (40) achieved 98% incorporation in *Caenorhabditis elegans* fed with *Escherichia coli* grown on medium enriched in ^{15}N. Metabolic labeling with ^{15}N is even better suited for labeling of plant cell cultures, which can be grown directly on a basal salt medium containing ^{15}N (or ^{14}N) as a sole nitrogen source. To test this, we grew *Arabidopsis* cell cultures in liquid medium containing ^{14}N or ^{15}N and analyzed isotope incorporation rates by MS. Four subculture periods of 7 days resulted in almost complete incorporation (>99%) of ^{15}N into randomly selected proteins (Fig. 2*b*).

To identify phosphorylated proteins involved in early elicitor signaling and defense response in *Arabidopsis*, we induced cells grown on ^{14}N-medium with flg22 or xylanase for 10 min and pooled the cells with an equal amount of ^{15}N-grown cells that where mock-treated. The pooled cells were homogenized, PM vesicles were purified, and phosphopeptides were isolated as described above. To obtain biologically relevant high confidence data, we also performed an inverse labeling experiment with elicitor induction of the ^{15}N-grown cells and mock treatment of the ^{14}N-grown cells for both elicitors. Individual SCX fractions enriched in phosphopeptides with titanium oxide were analyzed by LC-MS. Analysis of phosphopeptides by tandem MS is often hindered by the preferential loss of phosphoric acid upon fragmentation of precursor ions, often resulting in a predominant neutral loss ion $(M + nH^+ - H_3PO_4)^{n+}$. This hinders sequence annotation and prevents the identification of phosphopeptides and phosphorylation sites (as previously described (26)). To overcome these limitations we performed mass spectrometric analysis on an LTQ-FT-ICR mass spectrometer. Such an instrument provides several advantages when required to perform identification and localization of phosphorylated residues, including high dynamic range and mass accuracy as well as allowing multiple levels of tandem mass spectrometry. This latter feature allows the further sequencing of dominant neutral loss peak by MS^3. Recently MS^3 has been used to good effect to identify phosphorylated peptides in yeast (26). Each of our phosphopeptide-enriched samples was subjected to an LC-MS analysis that included MS^3 scans that were initiated when the neutral loss of phosphoric acid was detected. Analyses including MS^3 scans can significantly reduce the number of peptides that are sequenced during an LC run, and so to acquire the most comprehensive analysis of each sample a regular MS analysis was also performed. Fig. 3 shows an example of an MS analysis of a phosphopeptide with neutral loss-dependent MS^3 scan. The *left spectrum* shows an FT-ICR-MS scan containing the ^{14}N (824.88 *m/z*) and ^{15}N (836.34 *m/z*) peaks for RGNpSSNDHELGILR (where pS is phosphoserine) of RBOHD from an flg22 sample. From this spectrum the ratio between ^{14}N- and ^{15}N-labeled versions of the peptide can be determined; it reflects the relative level of phosphorylation in the flg22-treated culture (^{14}N) as compared with the mock-treated culture (^{15}N). The *middle spectrum* shows

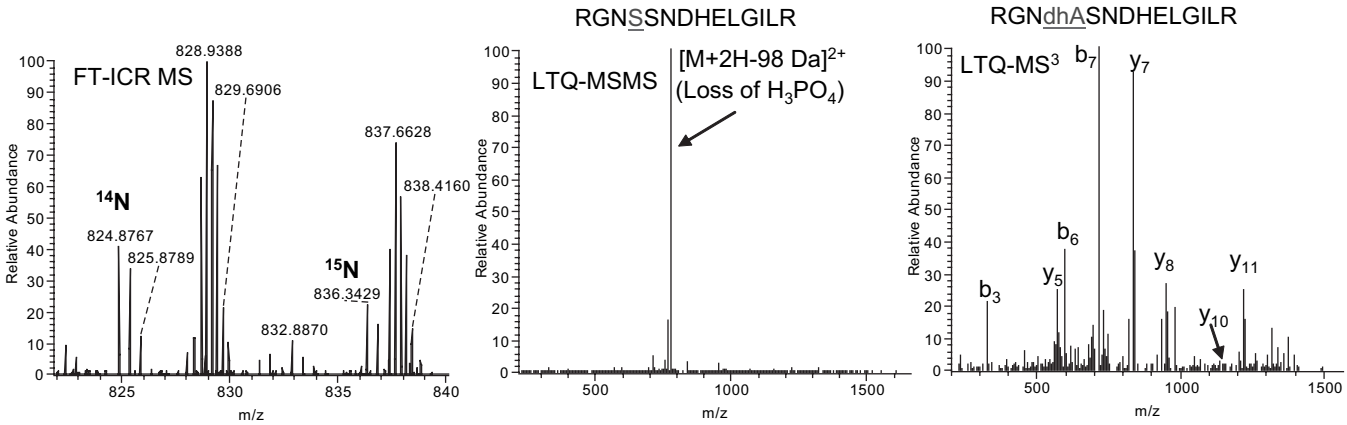

FIG. 3. **LTQ-FT neutral loss-dependent MS^3 scan of a phosphopeptide from RBOHD.** *Left*, FT-ICR mass spectrum containing the ^{14}N (824.88 *m/z*) and ^{15}N (836.34 *m/z*) peaks for RGNpSSNDHELGILR (of RBOHD, flg22 data set). *Middle*, MS/MS of ^{14}N precursor RGNpSSNDHELGILR, which contains a dominant phosphoric acid neutral loss (776.88 *m/z*). *Right*, MS^3 spectrum of neutral loss peak, which allows sequencing and identification of phosphorylation site. Note that in the MS^3 scan, phosphoserine has been modified into dehydroalanine (*dhA*) after neutral loss. Ions are assigned according to peptide fragmentation nomenclature as designated by Roepstorff and Fohlman (69).

the MS^2 of ^{14}N precursor ion (824.88 *m/z*) that was isolated and fragmented in the LTQ. The predominant mass in this spectrum corresponds to the neutral loss ion (775.94 *m/z*). The *right spectrum* shows the corresponding MS^3 after isolation and fragmentation of the neutral loss ion in the LTQ. From this spectrum the amino acid sequence and position of the phosphorylated residue (Ser at position 4) were determined. The corresponding ^{15}N peak was analyzed in an identical manner by independent MS^2 and MS^3 (data not shown) providing independent amino acid sequence information and annotation of the phosphorylated residue.

Membrane-associated Proteins Identified

A general survey of our flg22-induced and xylanase-induced data sets shows that we identified a total of 1186 *Arabidopsis* proteins from our plasma membrane-enriched fractions (Supplemental Table I). A little less then half of these were predicted to have at least one transmembrane domain (Fig. 4*a*). Comparison of the data with three other proteomics data sets obtained from purified plasma membrane vesicles isolated with aqueous two-phase partitioning (18, 32, 33) showed about 80% overlap with the data set that also used *Arabidopsis* suspension cells (155 of 192 reported proteins (18)). Membrane extracts from whole plants (32, 33) show only a 50% overlap with data presented here (169 of 304 and 54 of 104 proteins, respectively). A comparison against a recent large scale localization study of *Arabidopsis* organelle proteins showed an overlap of 170 proteins with our data set (41). Of these 170 proteins 39% were classified as PM, 25% were classified as endoplasmic reticulum, 4% were classified as Golgi, 2% were classified as vacuolar, and another 29% were not classified in this LOPIT (localization of organelle proteins by isotope tagging) analysis (41). Overall this comparison correlates well with the data presented in Fig. 2*a* and indicates that our samples are highly enriched in PM proteins. In addition to the observed overlap with these four published proteomics data sets (18, 32, 33, 41) we also identified a substantial number (808) of novel membrane-associated proteins. Despite the high level of enrichment of our plasma membrane preparations we, like Nuhse *et al.* (18), also did observe a small number of potential contaminants, such as DNA-binding proteins (Supplemental Table I).

In our data sets we identified a total of 1172 phosphopeptides (Fig. 4*b*), including 1011 new phosphopeptides, each with one or more phosphorylated residues. We observed a substantial overlap in identified phosphopeptides between our two data sets (Fig. 4*b*). Almost 60% of all phosphopeptides identified in the xylanase-treated cells were also found in the flg22-treated cells. However, there were also a considerable amount of phosphopeptides found in only one of the data sets. This is likely due to the fact that MS analysis of complex peptide samples is unlikely to give full coverage of all peptides in the mixture. Comparison of the data with another proteomics data set obtained from purified plasma membrane vesicles isolated with aqueous two-phase partitioning and selective phosphopeptide enrichment (18) also showed about 57% overlap (161 of 283 phosphopeptides) (Fig. 4*b*).

Elicitation-induced Changes in Protein Phosphorylation

10-min exposure of *Arabidopsis* cells to general elicitors resulted in significant induction of MAP kinase activity. With a short induction time we aimed to induce only post-translational modifications and expected to limit the contribution of transcription and translation to any observed changes in protein phosphorylation and protein abundance. We analyzed the changes in protein abundance by calculating the ratio of each peptide in the elicitor-treated samples *versus* mock-treated samples. A total of 16,196 peak pairs were compared using MSQuant (70), and a ratio of elicitor-treated *versus* mock-treated was determined for all of these. For 1069 peptides we

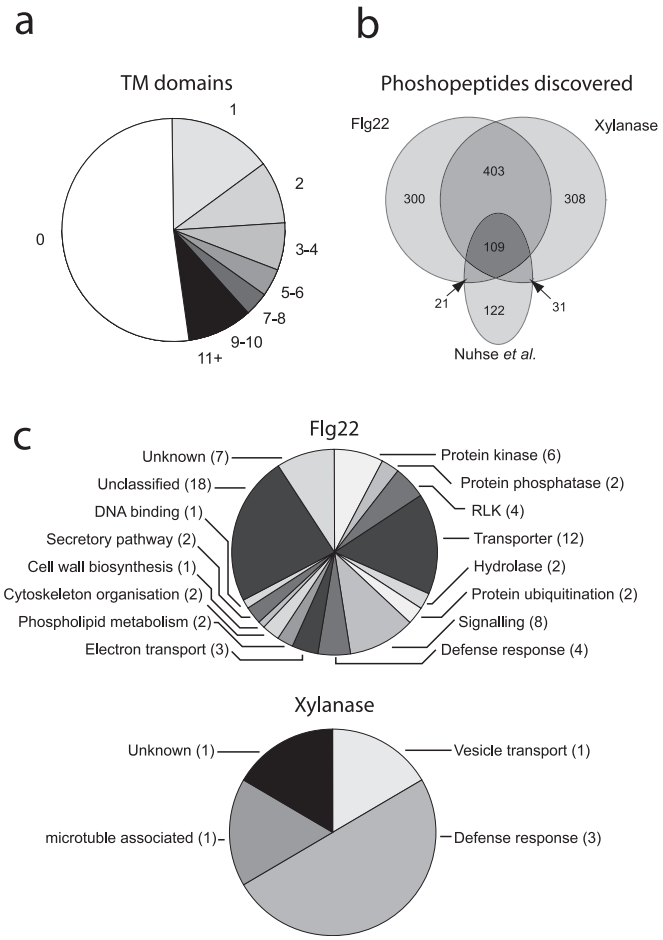

FIG. 4. **Protein classifications.** *a*, proportional representation of transmembrane domains within proteins found in this study as predicted by TMHMM (www.cbs.dtu.dk/services/TMHMM/). *b*, Venn diagram depicting the total number of unique phosphopeptides identified in data sets from xylanase and flg22 treatment experiments compared with the data set published by Nuhse *et al.* (18). *c*, representation of functional protein classes of PM phosphoproteins with significantly altered phosphorylation upon treatment with flg22 or xylanase. *TM*, transmembrane.

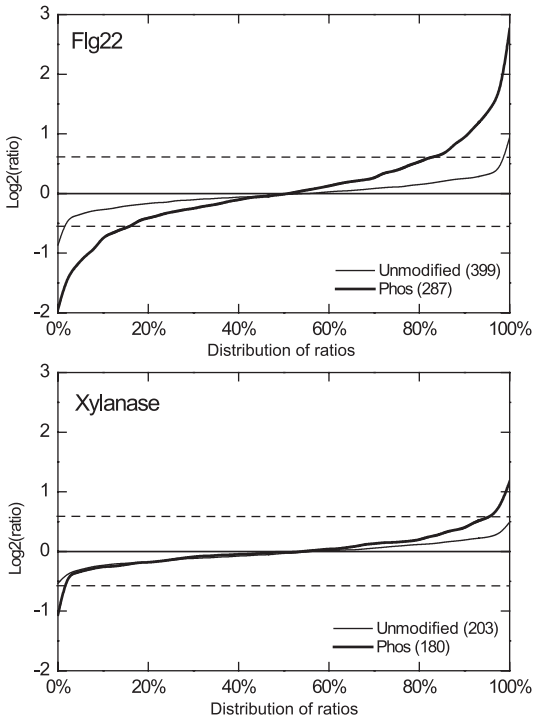

FIG. 5. **Ratio distribution of peptide ratios.** The average ratio for each peptide was log2-transformed and distributed in equally spaced bins according to the ratio. The average ratio for each bin is shown on the *y axis*, and the bins were ordered from low to high ratio on the *x axis*. The *top graph* shows all unmodified peptides and phosphopeptides (*Phos*) measured in both biological replicas of the flg22-treated cells. The *bottom graph* shows the same for the xylanase-treated cells.

were able to identify a ratio in both biological replicas, and 467 of these peptides had one or more phosphorylated residues. To identify proteins that were differentially phosphorylated in response to either flg22, xylanase, or both elicitors, we normalized the ratios of the non-phosphorylated peptides and phosphopeptides found in both biological replicas of the inverse labeling experiment (Fig. 5). As a result of the normalization, the average ratios of non-phosphorylated peptides in both data sets were distributed around 1. More than 96% of non-phosphopeptides (96% for flg22 and 100% for xylanase) had a ratio that remained within 3 standard deviations (ratio <0.67 or ratio >1.5) of the mean (Fig. 5).This indicates that at 10 min after elicitation only a very few proteins changed in abundance. We detected five proteins with a significant change in abundance in both replicas in the flg22 sample (Table I). As none of these proteins are obvious transmembrane proteins, the observed change in abundance is likely due to translocation to the plasma membrane or *de novo* protein synthesis. We presuppose that translocation of protein to or from the membrane is the major contributor to this phenomenon because dramatic increases in *de novo* protein synthesis are unprecedented at 10 min after addition of an elicitor. Translocation of cytosolic proteins to the membranes has been reported previously in response to both race-specific and general elicitors (42, 43). Our data suggest that translocation of these proteins to membranes is an immediate response that may be integral to elicitor signal transduction or elicitor-induced immediate defense response in plants. More importantly, our data showed that the overwhelming majority of the proteins present in both biological replicas show no changes in abundance at 10 min after induction with elicitors (Fig. 5).

The normalized average ratios of the phosphopeptides were also distributed around 1, but the fraction of phosphopeptides with a ratio that remained within 3 standard deviations of the mean (*i.e.* ratio <0.67 or ratio >1.5) was much smaller (Fig. 5), especially for the flg22 data set (66% for flg22 and 93% for xylanase). This data distribution, together with the data distribution of the non-phosphopeptides, suggested that the observed ratios for the phosphopeptides are

TABLE I
Identified proteins with differential abundance

The presented ratios and S.E. values were calculated by averaging $^{14}N/^{15}N$ ratios from consecutive FT-MS scans during the elution of the individual peptide pairs and by averaging data from two biological replicas. AGI_ID, *Arabidopsis* Gene Index number.

Treatment	AGI_ID	Ratio Treatment/mock	Annotation
flg22	At1g53840	2.56 ± 0.2	Pectinesterase family protein
flg22	At4g12070	2.08 ± 0.1	Expressed protein
flg22	At4g03080	1.84 ± 0.03	Kelch repeat-containing serine/threonine phosphoesterase family protein
flg22	At2g01340	0.55 ± 0.003	Expressed protein
flg22	At3g63260	0.53 ± 0.04	Protein kinase

almost entirely due to changes in phosphorylation status and not due to changes in protein abundance. This was further evaluated by comparing the ratios of the phosphopeptides to ratios of non-phosphopeptides from the same proteins when these were available. Of the 99 comparisons we were able to do, only three comparisons indicated that the observed differential ratio for the phosphopeptide could also have been due to an increase in protein abundance (Supplemental Table II). The three corresponding proteins (At3g26935, At2g17480, and At1g45688) were therefore not considered to be differentially phosphorylated. Together the distribution analysis and the ratio comparison show that the vast majority of differential ratios for the phosphopeptides are caused by differential phosphorylation of the corresponding proteins.

Differential Protein Phosphorylation

From our two data sets we identified 472 proteins that were phosphorylated on one or more residues. The majority of these proteins were not identified previously as phosphoproteins. When compared with the only other large scale protein phosphorylation analysis study (18) we found a significant number of proteins present in their data set that are also present as phosphoproteins in our data set. This was anticipated as Nuhse *et al.* (18) extracted phosphopeptides from uninduced cells combined with cells induced with flg22 for 8 min. However, these authors were unable to distinguish between phosphorylated residues from untreated and elicitor-induced cells. Using our metabolic labeling strategy we could identify one or more differentially phosphorylated residues in at least 98 phosphopeptides corresponding to 76 proteins (Table II). We considered peptides to be differentially phosphorylated when we were able to identify the corresponding phosphopeptides in both biological replicas and when these phosphopeptides had a normalized ratio that was at least 3 standard deviations away from the mean (ratio <0.67 or ratio >1.5; Fig. 6). These selection criteria (outlined in Fig. 6) were used to ensure that we obtained high confidence data sets with differentially phosphorylated peptides. A further measure of the confidence level of these data sets is the consistent reproducibility of the ratios in the two biological replicas as visualized in a *x-y* scatter plot (Fig. 7). Overall the ratios from biological replica 1 match the amplitude and direction of change of the ratios from biological replica 2 for both elicitor treatments with only a few outliers in each set. Furthermore this consistent reproducibility is also evident from the small S.E. values of the ratios in Table II. Functional classification of the differentially phosphorylated proteins identified a substantial number of proteins involved in signal transduction. These include ion channels, calcium ATPases, calmodulins, protein kinases, protein phosphatases, and receptor-like kinases (Fig. 4*c* and Table II).

A substantial number (12 of 76) of the differentially phosphorylated proteins are enzymes involved in protein phosphorylation/dephosphorylation, including members of different families of kinases, receptor-like kinases (RLKs) and protein phosphatases (Fig. 4*c*). Among these we could identify proteins that have been implicated previously in defense responses. One such example is Botrytis-Induced Kinase1 (BIK1; At2g39660), which codes a membrane-anchored protein kinase that was shown recently to be required for basal defense (44). In the present study we showed that this protein is phosphorylated on Ser-18 and dephosphorylated at Ser-28 in response to flg22, suggesting that the changes in phosphorylation status of these residues are important for elicitor-induced activation and by inference for basal defense.

Our screen identified at least three CDPKs (At1g18890, At5g19450, and At5g12480) that are differentially phosphorylated in response to flg22 (Table II and Supplemental Table III). Previously CDPKs have been shown be activated in response to fungal elicitors in french bean cells (45) and in *Nicotiana benthamiana* in response to race-specific elicitor (46). The fact that three different CDPKs were differentially phosphorylated in response to flg22 points to the central role this class of protein kinases plays in defense signal transduction. It is also interesting to note that four RLKs (At5g67200, At1g27190, At2g26730, and At4g03390) were differentially phosphorylated in response to flg22 (Table II). These four RLKs do not include FLS2 (At5g46330), the RLK that is required for flg22 perception. We did not identify any phosphopeptides corresponding to FLS2, although we did identify one non-phosphorylated FLS2 peptide in our data set. Phosphorylated FLS2 is rapidly internalized and degraded upon flg22 binding as recently described by Robatzek *et al.* (47). Perhaps this prevented detection of FLS2 phosphopeptides in

TABLE II

Identified differentially regulated phosphopeptides

The presented ratios and S.E. values were calculated by averaging $^{14}N/^{15}N$ ratios from consecutive FT-MS scans during the elution of the individual peptide pairs and by averaging data from two biological replicas. Capital letters in the peptide sequence column indicate amino acids, and lower case p indicates phosphorylation of the Ser or Thr residue that follows. Rows in gray indicate phosphopeptides up-regulated by xylanase as well as flg22. Phosphorylated residues were predicted by Mascot and manually validated. AGI_ID, *Arabidopsis* Gene Index number; pT, phosphothreonine.

AGI_ID	Peptide sequence	Ratio Xylanase / mock	Ratio Flg22 / mock	Locus	Annotation
At1g01540	ADFASAAIApTPPISK	0.82 ± 0.18	0.52 ± 0.04		protein kinase family protein
At1g05150	ADNNNNNVDAFpSDAGWSR		2.53 ± 0.15		calcium-binding EF hand family protein
At1g07630	SSGPIVLGpSGPIER		2.42 ± 0.05		protein phosphatase 2C family protein
At1g15210	NMEDIFNTp*[SS]*R	1.31 ± 0.37	2.27 ± 0.06		ABC transporter family protein
At1g16860	VSGPLDpSSGLMK	1.18 ± 0.03	1.74 ± 0.55		merozoite surface protein-related
At1g18390	SGPLVAQpSPDSVIVK	0.83 ± 0.07	0.51 ± 0.05		protein kinase family protein
At1g18890	SLpSINLMK	1.19 ± 0.08	2.51 ± 0.39	ATCDPK1	calcium-dependent protein kinase 1 (CDPK1)
At1g27190	HGVpSEHYDEFPLVFNK		1.61 ± 0.38		leucine-rich repeat transmembrane protein kinase
At1g30440	pSGGYVGGPNEGGGGGGGWATAVR	0.82 ± 0.09	1.83 ± 0.35		phototropic-responsive NPH3 family protein
At1g30690	SApSFKEESDFFADLK		1.53 ± 0.17		SEC14 cytosolic factor family
At1g33990	TLpSDPFSNGK		0.52 ± 0.05		hydrolase
At1g53590	KEEFLIGSIEEESQSQpSPR		1.95 ± 0.43		C2 domain-containing protein
At1g54610	ASSGVVVVGESpSVTK		5.36 ± 0.15		protein kinase family protein
At1g59610	AAAASSWSDNSGTESpSPR	2.05 ± 0.21		ADL3	dynamin-like protein
At1g59870	NIEDIFp*[SS]*GpSRR		1.53 ± 0.14	PEN3	ABC transporter family protein (PEN3)
At1g59870	NIEDIFSSGpSR	1.64 ± 0.05	2.37 ± 0.33	PEN3	ABC transporter family protein (PEN3)
At1g59870	NIEDIFSSGpSRR	1.51 ± 0.2	2.15 ± 0.13	PEN3	ABC transporter family protein (PEN 3)
At1g59870	TQpSVNDDEEALK	2.26 ± 0.4	3.14 ± 0.25	PEN3	ABC transporter family protein (PEN3)
At1g61250	LpSPLPPEPVGFDYGR		0.26 ± 0.06	SC3	secretory carrier membrane protein (SCAMP) family protein
At1g62320	p*[SS]*PVNSGAFVSK		0.55 ± 0.07		early-responsive to dehydration protein-related
At1g66480	TVpSDVTIGR		2.07 ± 0.06		expressed protein
At1g68720	VLPQEAPSLHQVEVGQTpSPR		2.12 ± 0.17		cytidine/deoxycytidylate deaminase family protein
At1g73590	FHYQSGGSGGGGGAHYPAPNPGMF pSPNTGGGGGTAAK		0.65 ± 0.09	PIN1	auxin efflux carrier protein
At1g73590	Gp*[SS]*FNHTDFYSMMASGGGR		1.54 ± 0.21	PIN1	auxin efflux carrier protein
At1g73590	GPTPRPpSNYEEDGGPAKPTAAGTAA GAGR		0.66 ± 0.11	PIN1	auxin efflux carrier protein
At1g76070	SDAVWDEPTpSPK	0.48 ± 0.26	0.37 ± 0.02		expressed protein
At1g76660	SEADLDSQVVDFQpSPK		1.87 ± 0.44		expressed protein
At1g77110	Dp*[TT]*PVAAIGK		0.43 ± 0.05	PIN6	auxin transport protein
At1g78610	GLTPVSEpSPRVSpTK	0.89 ± 0.05	0.66 ± 0.07		mechanosensitive ion channel domain-containing protein
At2g01680	AVpSDIKHEVQSQLLQNEK		1.56 ± 0.09		ankyrin repeat family protein
At2g15760	p*[TS]*FSAADELFDGGK		0.38 ± 0.01		Calmodulin-binding protein
At2g18960	GLDIDTAGHHYpTV	0.94 ± 0.18	0.33 ± 0.01	AHA1	ATPase 1
At2g20840	YQSHpSFDDGEINPFANPTSVPAATS K		0.52 ± 0.04		secretory carrier membrane protein (SCAMP) family protein
At2g23140	pSGPLAATTSAATR		2.38 ± 0.39		armadillo/beta-catenin repeat family protein
At2g26730	GSEGQTPPGEpSRTPPR		0.59 ± 0.04		leucine-rich repeat transmembrane protein kinase

TABLE II—*continued*

AGI_ID	Peptide sequence	Ratio Xylanase / mock	Ratio Flg22 / mock	Locus	Annotation
At2g28070	MNSGSMApSPPVPEGGAGTGVVR		0.62 ± 0.07		ABC transporter family protein
At2g32450	VDNNNVDAFSEAGWpSR	1.01 ± 0.01	2.14 ± 0.37		calcium-binding EF hand family protein
At2g33490	VSSpSPTASPTFVSTPK	0.78 ± 0.1	0.39 ± 0.08		hydroxyproline-rich glycoprotein family protein
At2g35350	GATpSGPLDPPAGEISR	1.12 ± 0.01	1.55 ± 0.23		protein phosphatase 2C family protein
At2g35350	SGLFMpSGPIER	1.46 ± 0.22	3.09 ± 0.16		protein phosphatase 2C family protein
At2g36330	TMPSMpSPSSVSTEK		0.46 ± 0.02		integral membrane protein
At2g36910	FTHTQVIGMTSGSp*[SS]*R	1.32 ± 0.26	1.53 ± 0.07	ATPGP1	multidrug resistance P-glycoprotein
At2g38480	TSEPpTPASGTSTITQR		0.48 ± 0.05		integral membrane protein
At2g39660	p*[SS]*DLYGLSLSSR		2.28 ± 0.14	BIK1	protein kinase
At2g39660	SSDLYGLSLpSSR	1.03 ± 0.15	0.35 ± 0.04	BIK1	protein kinase
At2g43680	GASPQAISpSKPPpSPR		2.16 ± 0.22		calmodulin-binding family protein
At2g43680	GASPQAISSKPPpSPR	1.47 ± 0.27	1.87 ± 0.12		calmodulin-binding family protein
At2g43680	LDAPRPpTTPKPPpSPR	1.26 ± 0.01	1.54 ± 0.18		calmodulin-binding family protein
At2g43680	SLpSPKPPpSPR		1.58 ± 0.08		calmodulin-binding family protein
At2g43680	TLSPKPPpSPR		1.81 ± 0.17		calmodulin-binding family protein
At2g45820	ALAVVEKPIEEHpTPK		3.26 ± 0.26		DNA-binding protein
At2g45820	VDVEpSPAVLAPAKEPTPAPVEVADEK		1.77 ± 0.46		DNA-binding protein
At3g05200	TNpSLLVLPR		3.74 ± 0.57	ATL6	zinc finger family protein (ATL6)
At3g07540	SLFLSSTSApSPAR	0.77 ± 0.01	0.43 ± 0.04		formin homology 2 domain-containing protein
At3g09070	ApSWDGSLIGR		0.64 ± 0.07		glycine-rich protein
At3g17650	TSFpTLEEDPHASPLSPK		1.52 ± 0.01		oligopeptide transporter OPT family protein
At3g22180	NYDETGpSQLQASPSVVSR	0.85 ± 0.07	0.52 ± 0.07		zinc finger (DHHC type) family protein
At3g27390	KDEEPTPFpSGPVPR		6.8 ± 1.21		expressed protein
At3g28345	SSpSANSVTGPSTIK		0.61 ± 0.02		ABC transporter family protein
At3g28850	SFpSFDVGPNGGK	0.85 ± 0.01	0.52 ± 0		glutaredoxin family protein
At3g29360	FDWDHPLHLQPMpSPTTVK		1.82 ± 0.23		UDP-glucose 6-dehydrogenase
At3g46290	FEESpSIDDLSGVSMSK		1.73 ± 0.04		protein kinase
At3g48760	TVNGGMSpSPSLQK		0.65 ± 0.09		zinc finger (DHHC type) family protein
At4g03390	VTVMPIIpSPERPVK	1.42 ± 0.41	0.62 ± 0.04		leucine-rich repeat transmembrane protein kinase
At4g08330	APEYALVTQNpSDPTSPR	0.88 ± 0	0.63 ± 0.05		expressed protein
At4g13510	HGGFAYMYFDDDEpSHK		3.28 ± 1.45	AMT1	ammonium transporter 1
At4g19930	VPpSFIQR	1.13 ± 0	1.51 ± 0.13		F-box family protein
At4g24630	QpTPSVQIPR		0.56 ± 0.02		zinc finger (DHHC type) family protein
At4g29900	GEDKDVEAGpTSSFTEYEDSPFDIASTK	1.21 ± 0.2	1.84 ± 0.39	ACA10	calcium-transporting ATPase
At4g30190	GLDIETPpSHYTV	1 ± 0.13	0.47 ± 0.06	AHA2	ATPase 2
At4g32410	NAISpSPYIDPR	0.81 ± 0.03	0.4 ± 0	CESA1	cellulose synthase
At5g02620	SSPASMMpSDPELADSK	0.88 ± 0.13	0.63 ± 0.01		ankyrin repeat family protein
At5g03700	NLGSDpSFNSVEMSR	0.89 ± 0.29	0.27 ± 0.11		PAN domain-containing protein
At5g05170	HTDp*[ST]*VPVFNLDDIEEGVEGAGFDDEK		0.63 ± 0.21	CESA3	cellulose synthase
At5g05170	QDTSGEFSAApSPER		0.6 ± 0.04	CESA3	cellulose synthase

TABLE II—*continued*

AGI_ID	Peptide sequence	Ratio Xylanase / mock	Ratio Flg22 / mock	Locus	Annotation
At5g10470	SMAVSTQVLpSPSLR	2.01 ± 0.01			kinesin motor protein-related
At5g12080	pSVGSPAPVTPSK		2.58 ± 0.28		mechanosensitive ion channel domain-containing protein
At5g12080	SVGpSPAPVTPSK		0.66 ± 0.02		mechanosensitive ion channel domain-containing protein
At5g12480	NNPFYpSNEYATTDR	1.09 ± 0.09	1.5 ± 0.04	CPK7	calmodulin-domain protein kinase isoform 7
At5g23450	KQApSSELFSVPIDTPPELVFR		2.06 ± 0.21	ATLCBK1	diacylglycerol kinase family protein
At5g39865	GGLpSPVIVPR		0.36 ± 0.07		glutaredoxin family protein
At5g40300	QDQSpSPINFEMSSR	0.96 ± 0.03	0.39 ± 0.02		integral membrane protein
At5g41620	AVpTPSSSLEFR	0.99 ± 0.19	1.69 ± 0.45		expressed protein
At5g47910	GAFpSGPLGRPK	1.76 ± 0.29	3.07 ± 0.53	RBOHD	respiratory burst oxidase protein D
At5g47910	ILpSQMLSQK	2.06 ± 0.26	5.52 ± 1.07	RBOHD	respiratory burst oxidase protein D
At5g47910	RPpSPAVR		3.2 ± 0.16	RBOHD	respiratory burst oxidase protein D
At5g47910	TSpSAAIHALK	1.66 ± 0.11	3.72 ± 0.4	RBOHD	respiratory burst oxidase protein D
At5g48800	INpSGALSATMSPK	1.12 ± 0.04	2.87 ± 0.15		phototropic-responsive NPH3 family protein
At5g48800	INSGALSATMpSPK	0.79 ± 0.02	0.47 ± 0.04		phototropic-responsive NPH3 family protein
At5g50020	QpTPTVQIPR		0.44 ± 0.04		zinc finger (DHHC type) family protein
At5g61740	QNpSENVLIDMEK	1.29 ± 0.07	1.6 ± 0.31	ATATH14	ABC transporter family protein
At5g65660	LTVDVQpTPPQpSPPVKPAR		2.09 ± 0.42		hydroxyproline-rich glycoprotein family protein
At5g67200	IPNpSGNLVFCGESR	1.03 ± 0.02	1.69 ± 0.43		leucine-rich repeat transmembrane protein kinase
At5g67470	FGSAPTTAASRpSPEMK		0.61 ± 0.01		formin homology 2 domain-containing protein

our study and resulted in detection of unmodified FLS2 only. However, it is equally likely that we could not detect the FLS2 phosphopeptides due to incomplete (phospho-)peptide coverage. Nevertheless what could be the significance of the observed increased phosphorylation of multiple other RLKs? By phosphorylating multiple RLKs in response to the perception of flg22, the cell may prepare for the perception of other general elicitors and go into a primed state that will allow a faster defense response resulting in enhanced resistance. flg22 was recently shown to induce enhanced resistance to *P. syringae* pv. *tomato* DC3000 in *Arabidopsis* plants with a functional FLS2 protein (5). Priming of basal defense has been described previously for resistance induced by root-colonizing non-pathogenic pseudomonads in *Arabidopsis* (48, 49). Several bacterial determinants inducing induced systemic resistance-like resistance in *Arabidopsis* have been described previously and include lipopolysaccharide and flagellin isolated from induced systemic resistance-inducing pseudomonads (50). However the molecular mechanism behind this priming for enhanced resistance has so far not been elucidated. We postulate that perception of a general elicitor like flg22 induces local priming through the phosphorylation of multiple RLKs resulting in enhanced RLK-mediated detection of pathogens that ultimately leads to the described enhanced defense response (5).

Other proteins that were differentially phosphorylated and have an established link with defense response include the respiratory oxidative burst proteins RBOHD, ABC transporter PEN3 (At1g59870), and cellulose synthase CESA3 (At5g05170). Most proteins identified as differentially phosphorylated in this study, however, have no known link with defense responses or have been characterized previously to be involved in other signaling pathways or responses. Among these are a number of proteins that are involved in mediating auxin response, including PIN1 (At1g73590), PIN6 (At1g77110), AIR9 (At2g34680), and ABC transporter PGP1 (At2g36910). From our data it is not apparent what the physiological significance of the differential phosphorylation of these proteins is; however, recently flg22 has been shown to modulate auxin response. In *Arabidopsis* suspension cells and seedlings a 60-min induction with flg22 has been shown to cause down-regulation of many auxin signaling-related genes (6). Furthermore down-regulation of auxin signaling was shown to enhance resistance to virulent *Pseudomonas*, suggesting that down-regulation of the auxin signaling is part of the plant immune response (51). It was suggested by the authors that flg22-mediated down-regulation of auxin responses could be responsible for the flg22-induced growth inhibition in *Arabidopsis* seedling roots (3). It has been re-

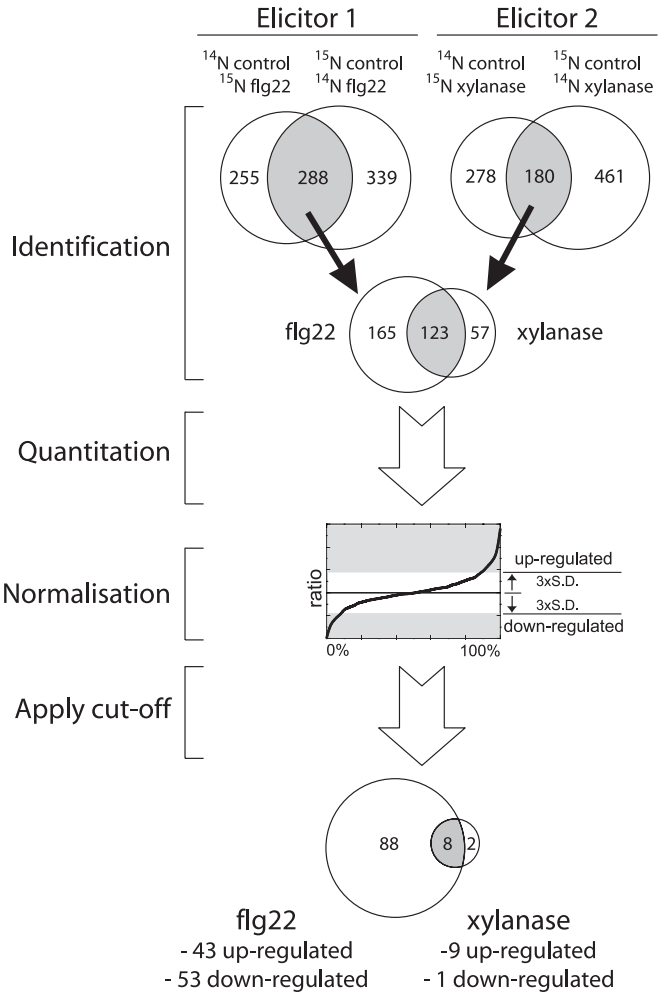

FIG. 6. **Selection criteria for differential phosphorylation sites.** A flow diagram shows the stringent selection of differential phosphorylation sites from the phosphopeptide data sets of both biological replicas. Phosphorylation sites that were identified in both biological replicas were selected, and the corresponding ratio between the light and heavy isotope isoforms of the phosphopeptides was determined. The data were subsequently normalized, and differential up- or down-regulation was determined by applying a cutoff that was 3 standard deviations (*3×S.D.*) away from the normalized mean ratio of 1.

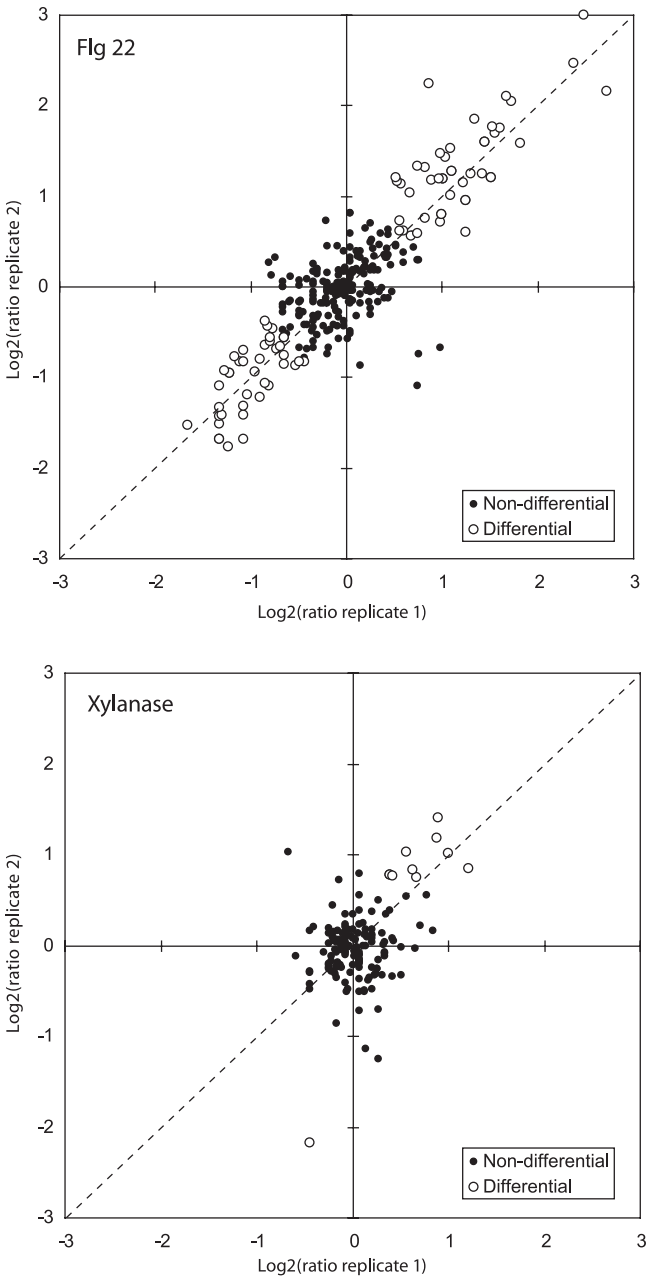

FIG. 7. **Correlation of the relative quantification of phosphorylation of individual peptides between biological replicas.** Shown are *x-y* scatter plots of the ratios (elicitor-treated/mock-treated) for all phosphopeptides for which two biological repeats were observed. Data are shown separately for the two elicitor treatments. *x value*, log (base 2)-transformed ratio for replicate 1 (^{14}N elicitor-treated sample, ^{15}N mock-treated sample). *y value*, log (base 2)-transformed ratio for replicate 2 (^{15}N elicitor-treated sample, ^{14}N mock-treated sample). Phosphopeptides considered to be significantly differentially phosphorylated are shown as *open circles*; non-differentially phosphorylated peptides are shown as *solid dots*. The *dotted line* shows maximum correlation between *x* and *y* values ($y = ax + b$, $a = 1$, $b = 0$).

ported previously that activation of a MAPK pathway involving MAPK kinase kinase NPK1 and unidentified MAPKs negatively regulates auxin-responsive gene expression in *Arabidopsis* (52). Because flg22 induces the activation of multiple MAPK activities, the differentially phosphorylated auxin response proteins may be direct or indirect targets of MAP kinases. MAP kinases phosphorylate serine or threonine residues followed by a proline in both plant and animal systems (53, 54). Three of the differentially phosphorylated auxin signaling proteins (PIN1, PIN6, and AIR9) have phosphorylated Ser or Thr residues followed by Pro (Table II and Supplemental Table III), suggesting that these proteins may qualify as direct MAPK targets. Thus, MAPK-dependent flg22-induced phosphorylation of one or more of these auxin signaling proteins could possibly play a role in the negative regulation of auxin signaling in *Arabidopsis* to enhance the plants immune response.

In addition to the elicitor-induced phosphorylation de-

scribed above we also detected elicitor-induced dephosphorylation of a substantial number of proteins. Most notably, two H^+-ATPases (At2g18960 and At4g30190) showed a 2-fold reduction in phosphorylation upon flg22 treatment. Furthermore two cellulose synthase proteins, CESA1 and CESA3 (At4g32410 and At5g05170), were also dephosphorylated in response to flg22 (Table II). In almost all of these proteins, other non-phosphorylated peptides were also detected and showed no change in abundance (Supplemental Table II), indicating that these proteins are dephosphorylated in response to elicitor. Previously a reduction in CESA3 levels or CESA3 activity was shown to induce jasmonate and ethylene accumulation and invoke defense gene expression in *Arabidopsis* (55, 56) linking reductions in cellulose synthesis to defense responses. Because perception of flg22 also induces the deposition of callose in *Arabidopsis* seedlings (3) the observed dephosphorylation of CESA proteins could indicate that the modulation of cellulose synthesis is related to a switch to defensive callose synthesis.

Overlap in flg22- and Xylanase-induced Phosphorylation

We detected 76 proteins in both biological replicas that showed differential phosphorylation upon treatment with either xylanase or flg22. Significantly three of the six proteins that were differentially phosphorylated in response to xylanase were also differentially phosphorylated in response to flg22 (Table II, highlighted in gray). An additional 53 proteins were identified that were potentially differentially phosphorylated in response to xylanase, and 19 of these were also potentially differentially phosphorylated in response to flg22 (Supplemental Table III). However, the corresponding 61 phosphopeptides could not be verified in both biological replicas. This could be due to technical limitations as MS analysis of complex peptide mixtures results in partial coverage of the sample and preferential detection of some peptides but not others. However, two of the three differentially phosphorylated proteins (PEN3 and RBOHD) have well established links to defense responses, and their differential phosphorylation in response to both elicitors indicates their conserved function in different defense signal transduction cascades. The ABC transporter PEN3 was originally isolated as a mutant locus that permitted penetration and infection by non-adapted fungi (57). This protein was differentially phosphorylated on two residues in response to both elicitors. Significantly a related ABC transporter (At1g15210) was also differentially phosphorylated in response to flg22 on an almost identical location. Recently it has been suggested that PEN3/PDR8 protein functions to export toxic compounds at the site of pathogen infection (58), and the phosphorylation sites we identified here may very well be involved in the activation of PEN3-like ABC transporters in response to general elicitor perception.

Elicitor-induced Differential Phosphorylation of Proteins Involved in Defense Responses

Oxidative Burst Proteins—The majority of the differentially phosphorylated proteins we identified have no experimentally defined function. However, a small number of the proteins we identified as differentially phosphorylated in response to flg22 or xylanase have been described previously as required for defense signaling or defense response. One of these proteins is the respiratory oxidative burst protein RBOHD. Respiratory oxidative burst is defined as the production of apoplastic reactive oxygen intermediates (ROIs), which is mediated by NADPH oxidases and apoplastic peroxidase, and is a hallmark of successful pathogen recognition in plants (16, 59, 60). NADPH oxidases, represented in a small family in *Arabidopsis* (*AtRbohA–J*), are implicated as one of the sources of ROI production. *Rboh* genes are transcriptionally up-regulated upon pathogen attack, and antisense reduction of RBOH in *Nicotiana* led to reduced production of ROIs and higher susceptibility to infection. Although ROIs were originally proposed to orchestrate cell death upon infection (61), recent evidence showed that mutations in *AtRbohD* and *AtRbohF*, required for ROI production in *Arabidopsis* leaves, have only a small effect on the hypersensitive response, and ROI production can even suppress cell death rather than induce it (59, 62).

In response to flg22, *Arabidopsis* leaves with functional FLS2 produce reactive oxygen species within minutes, and this oxidative burst peaks around 10 min (3). In response to a 10-min incubation with flg22 and xylanase we observed phosphorylation on seven different residues in RBOHD (Fig. 8*a*), three of which showed increased phosphorylation upon xylanase and flg22 treatment. As multiple non-phosphorylated peptides were also detected for this protein, the changes in phosphorylation can safely be attributed to phosphorylation rather than increased amount of protein. In general, both elicitors induce phosphorylation at similar locations, although flg22 tends to induce a stronger quantitative phosphorylation. These data show that RBOHD is very tightly regulated by phosphorylation as many residues were differentially phosphorylated in response to flg22 or xylanase, and three residues were differentially phosphorylated in response to both. A further four potential differentially phosphorylated residues were identified in one biological replica (Supplemental Table III) but could not be verified in the other biological replica. Detailed characterization of RBOHD point mutation versions of the protein expressed in a rbohd mutant background will be required to fully characterize the significance of the differentially phosphorylated residues in response to general elicitors or pathogen infection. Because there are multiple residues in RBOHD that become quantitatively phosphorylated in response to general elicitors it is likely that the activity of RBOHD is regulated by several different kinases acting in sequential or parallel pathways activated in response to general elicitor perception.

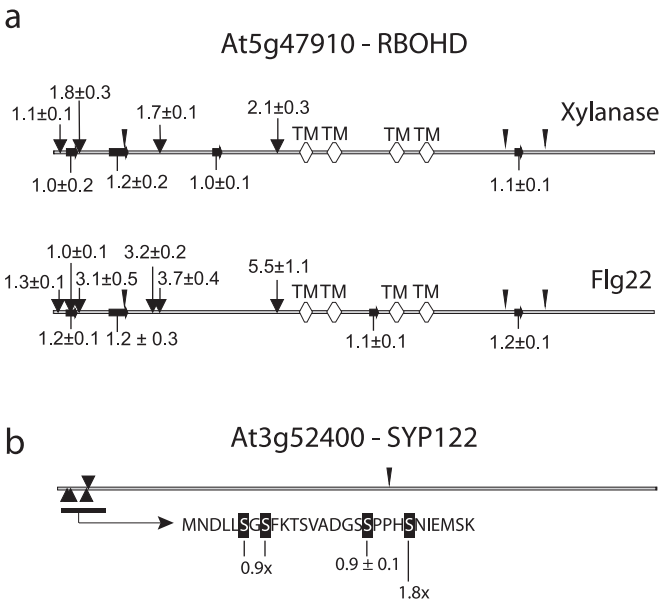

FIG. 8. **Differentially phosphorylated defense response proteins.** *a*, schematic representation of identified locations of phosphorylation on the respiratory burst oxidase protein RBOHD. *White diamonds* indicate transmembrane regions (*TM*). *Block arrows* indicate peptides without modifications. *Triangles* indicate differentially phosphorylated residues. *Numbers* indicate average and S.E. of the difference in abundance of the ^{14}N and ^{15}N signals from the peptide containing the phosphorylation site. *b*, schematic representation of identified locations of phosphorylation on the syntaxin SYP122. *Triangles* represent phosphorylated residues. *Numbers* indicate average and S.E. of the difference in abundance of the ^{14}N and ^{15}N signals from the peptide containing the phosphorylation site.

Syntaxins and Other Vesicle Traffic-related Proteins—Another class of proteins associated with defense response and differentially phosphorylated in response to flg22 is syntaxins. Syntaxin SYP121 (At3g11820), also known as PEN1, is required for non-host resistance against non-adapted fungi. Non-host resistance to non-adapted fungi was shown recently to be comprised of pre- and postinvasion defense (63). The postinvasion defense is dependent on the EDS1-PAD4-SAG101 signaling complex, whereas preinvasion defensive layers where shown to require PEN1, PEN2, and PEN3. Lipka *et al.* (63) suggested that both preinvasion defense and postinvasion defense are probably inducible upon pathogen perception and may be mediated through pathogen-associated molecular pattern or general elicitor receptors. This was in part based on the observation that *PEN1*, *PEN2*, and *PEN3* expression is induced in response to flg22 perception (5). Our data on differential phosphorylation of ABC transporter PEN3/PDR8 in response to both flg22 and xylanase suggest that preinvasion defense may also be regulated at the post-translational level. Furthermore we found that SYP121/PEN1 is also phosphorylated on the N terminus (Ser-7) upon flg22 treatment (Supplemental Table III; 1.3-fold increase but statistically significant when corrected for the ratios of other peptides from the same protein, $p < 0.01$). Phosphorylation of the same peptide was not increased upon xylanase treatment (ratio of 1.1). For a related syntaxin, SYP122 (At3g52400), we identified three phosphorylated peptides with a total of four phosphorylation sites in the flg22-treated cells (Fig. 8*b*). Syntaxin SYP122 was shown previously to be phosphorylated on a specific residue (Ser-18) in response to flg22 treatment (64). We also observed a differentially phosphorylated peptide in which two residues (Ser-18 and Ser-22) were phosphorylated (ratio of 1.8; Supplemental Table III). In addition, we also observed a phosphopeptide in which only Ser-18 was phosphorylated, but this peptide did not have a differential ratio (0.85). This suggests that, under our conditions, Ser-18 may not be differentially phosphorylated in response to flg22 but that it is Ser-22 that becomes phosphorylated in response to flg22.

SYP121 and SYP122 encode soluble *N*-ethylmaleimide-sensitive factor attachment protein receptor (SNARE) domain-containing and plasma membrane-resident syntaxins, which become recruited into plasma membrane microdomains beneath incipient fungal entry sites (65, 66). PEN1 was originally isolated as a mediator in fungal penetration and was reported recently to have a basal function in secretion and a specialized defense-related function (57, 65). Because SNARE proteins play a key role in vesicle trafficking in eukaryotic cells, these findings have been interpreted as evidence for the existence of a vesicle-associated resistance mechanism preventing powdery mildew ingress (63). In addition to SYP121 and SYP122 we also identified other proteins involved in vesicle transport to be differentially phosphorylated in response to flg22 and or xylanase. Both elicitors induced phosphorylation of a kinesin motor protein (At5g10470) (Table II and Supplemental Table III), and a second kinesin (At1g21730) was also phosphorylated in response to xylanase treatment (Supplemental Table III). Kinesin motor proteins have been described to be involved in vesicle transport along microtubules (67). Furthermore the dynamin-like protein ADL3 (At1g59610) was also phosphorylated in response to xylanase (Table II), and ADL6 (At1g10290) was phosphorylated in response to flg22 (Supplemental Table III). Dynamins are mechanochemical GTPases that form multimeric rings around the necks of budding clathrin-coated vesicles (Ref. 68 and references therein).

Taken together, the data on differential phosphorylation of vesicle transport-associated proteins implicate vesicle traffic as an important response upon general elicitor perception, and some of these proteins may turn out to be part of the preinvasive defensive layer described by Lipka *et al.* (63). The recently reported ligand-induced endocytosis of the receptor FLS2 (47) further illustrates the importance of vesicle traffic in elicitor-induced responses. flg22 binding induces the internalization of FLS2 and its subsequent degradation, and this process is dependent on protein kinase activity. We did not observe any changes in FLS2 protein abundance (ratio of 1.0) in our experiments, but this may be due to the earlier time

point (10 min) we chose as compared with the earliest time (20–40 min) reported for FLS2 internalization (47). However, our combined data point to the phosphorylation-dependent regulation of endocytosis and vesicle traffic in response to general elicitor perception.

Conclusion

Using a stable isotope metabolic labeling strategy combined with selective purification of phosphopeptides and LC-MS/MS we were able to identify a large number of protein phosphorylation events in *Arabidopsis* cells. With this newly established method we identified novel phosphorylation sites in many PM-associated proteins and showed that some of these are differentially phosphorylated in response to general elicitors. These differentially phosphorylated proteins are all potential new signal transduction components or early response regulators and provide a wealth of information on early signaling and response in *Arabidopsis* cells. Functional analysis of these proteins by site-directed mutagenesis of the identified phosphorylation residues or reverse genetic approaches will now be required to validate their role in elicitor signaling. Our strategy can also be applied to other stress conditions or responses to environmental changes to identify possible early signal transduction proteins thereby elucidating other signal transduction networks in plants. Our study has provided the largest quantitative *Arabidopsis* phosphoproteomics data set to date and reveals that the plant's early response at the protein level is primarily at the level of post-translational modifications. By just zooming in on (de-)phosphorylation the data set reveals that the response to an elicitor by the plant is a complex multifaceted interplay of many signaling pathways, indicating that a comprehensive system biology approach is needed to understand the full mechanism. Quantitative phosphoproteomics as described in this study is a novel tool that can complement ongoing genomics and reverse genetic approaches to identify the molecular mechanism of regulation of newly discovered and established plant signal transduction components and early response proteins.

Acknowledgments—We thank Joost Gouw for modifications to MSQuant, Ken-ichiro Shimazaki for the VHA1 antibody, Masayoshi Maeshima for the VVP2 antibody, John C. Rogers for the tonoplast intrinsic protein antibody, Jim Whelan for the uncoupling protein antibody, Jeffrey Harper for the ACA-2p antibody, Sharon Mithoe for help with Western blotting, and Johan Memelink for critically reading the manuscript.

* This work was supported by a Horizon Breakthrough grant from the National Genomics Initiative (NROG, The Hague, The Netherlands) (to F. L. H. M.) and by The Netherlands Proteomics Centre (Utrecht, The Netherlands). The costs of publication of this article were defrayed in part by the payment of page charges. This article must therefore be hereby marked "*advertisement*" in accordance with 18 U.S.C. Section 1734 solely to indicate this fact.

S The on-line version of this article (available at http://www.mcponline.org) contains supplemental material.

§ Both authors contributed equally to this work.

¶Present address: Dept. for Physiological Chemistry, University Medical Center Utrecht, Universiteitsweg 100, 3584 CG Utrecht, The Netherlands.

** To whom correspondence may be addressed. E-mail: m.slijper@pharm.uu.nl.

‡‡ To whom correspondence may be addressed. E-mail: f.l.h.menke@bio.uu.nl.

REFERENCES

1. Nurnberger, T., Brunner, F., Kemmerling, B., and Piater, L. (2004) Innate immunity in plants and animals: striking similarities and obvious differences. *Immunol. Rev.* **198,** 249–266
2. Asai, T., Tena, G., Plotnikova, J., Willmann, M. R., Chiu, W. L., Gomez-Gomez, L., Boller, T., Ausubel, F. M., and Sheen, J. (2002) MAP kinase signalling cascade in Arabidopsis innate immunity. *Nature* **415,** 977–983
3. Gomez-Gomez, L., Felix, G., and Boller, T. (1999) A single locus determines sensitivity to bacterial flagellin in Arabidopsis thaliana. *Plant J.* **18,** 277–284
4. Nuhse, T. S., Peck, S. C., Hirt, H., and Boller, T. (2000) Microbial elicitors induce activation and dual phosphorylation of the Arabidopsis thaliana MAPK 6. *J. Biol. Chem.* **275,** 7521–7526
5. Zipfel, C., Robatzek, S., Navarro, L., Oakeley, E. J., Jones, J. D., Felix, G., and Boller, T. (2004) Bacterial disease resistance in Arabidopsis through flagellin perception. *Nature* **428,** 764–767
6. Navarro, L., Zipfel, C., Rowland, O., Keller, I., Robatzek, S., Boller, T., and Jones, J. D. (2004) The transcriptional innate immune response to flg22. Interplay and overlap with Avr gene-dependent defense responses and bacterial pathogenesis. *Plant Physiol.* **135,** 1113–1128
7. Tao, Y., Xie, Z., Chen, W., Glazebrook, J., Chang, H. S., Han, B., Zhu, T., Zou, G., and Katagiri, F. (2003) Quantitative nature of Arabidopsis responses during compatible and incompatible interactions with the bacterial pathogen Pseudomonas syringae. *Plant Cell* **15,** 317–330
8. Martin, G. B., Brommonschenkel, S. H., Chunwongse, J., Frary, A., Ganal, M. W., Spivey, R., Wu, T., Earle, E. D., and Tanksley, S. D. (1993) Map-based cloning of a protein kinase gene conferring disease resistance in tomato. *Science* **262,** 1432–1436
9. Song, W. Y., Wang, G. L., Chen, L. L., Kim, H. S., Pi, L. Y., Holsten, T., Gardner, J., Wang, B., Zhai, W. X., Zhu, L. H., Fauquet, C., and Ronald, P. (1995) A receptor kinase-like protein encoded by the rice disease resistance gene, Xa21. *Science* **270,** 1804–1806
10. Jin, H., Axtell, M. J., Dahlbeck, D., Ekwenna, O., Zhang, S., Staskawicz, B., and Baker, B. (2002) NPK1, an MEKK1-like mitogen-activated protein kinase kinase kinase, regulates innate immunity and development in plants. *Dev. Cell* **3,** 291–297
11. Menke, F. L., van Pelt, J. A., Pieterse, C. M., and Klessig, D. F. (2004) Silencing of the mitogen-activated protein kinase MPK6 compromises disease resistance in Arabidopsis. *Plant Cell* **16,** 897–907
12. Felix, G., Duran, J. D., Volko, S., and Boller, T. (1999) Plants have a sensitive perception system for the most conserved domain of bacterial flagellin. *Plant J.* **18,** 265–276
13. Menke, F. L., Parchmann, S., Mueller, M. J., Kijne, J. W., and Memelink, J. (1999) Involvement of the octadecanoid pathway and protein phosphorylation in fungal elicitor-induced expression of terpenoid indole alkaloid biosynthetic genes in Catharanthus roseus. *Plant Physiol.* **119,** 1289–1296
14. Chivasa, S., Hamilton, J. M., Pringle, R. S., Ndimba, B. K., Simon, W. J., Lindsey, K., and Slabas, A. R. (2006) Proteomic analysis of differentially expressed proteins in fungal elicitor-treated Arabidopsis cell cultures. *J. Exp. Bot.* **57,** 1553–1562
15. Ndimba, B. K., Chivasa, S., Hamilton, J. M., Simon, W. J., and Slabas, A. R. (2003) Proteomic analysis of changes in the extracellular matrix of Arabidopsis cell suspension cultures induced by fungal elicitors. *Proteomics* **3,** 1047–1059
16. Bindschedler, L. V., Dewdney, J., Blee, K. A., Stone, J. M., Asai, T., Plotnikov, J., Denoux, C., Hayes, T., Gerrish, C., Davies, D. R., Ausubel, F. M., and Paul Bolwell, G. (2006) Peroxidase-dependent apoplastic oxidative burst in Arabidopsis required for pathogen resistance. *Plant J.* **47,** 851–863
17. Scheel, D. (1998) Resistance response physiology and signal transduction. *Curr. Opin. Plant Biol.* **1,** 305–310

18. Nuhse, T. S., Stensballe, A., Jensen, O. N., and Peck, S. C. (2004) Phosphoproteomics of the Arabidopsis plasma membrane and a new phosphorylation site database. *Plant Cell* **16,** 2394–2405
19. Peck, S. C., Nuhse, T. S., Hess, D., Iglesias, A., Meins, F., and Boller, T. (2001) Directed proteomics identifies a plant-specific protein rapidly phosphorylated in response to bacterial and fungal elicitors. *Plant Cell* **13,** 1467–1475
20. Hunter, T. (1998) The Croonian Lecture 1997. The phosphorylation of proteins on tyrosine: its role in cell growth and disease. *Philos. Trans. R. Soc. Lond. B Biol. Sci.* **353,** 583–605
21. Steen, H., Jebanathirajah, J. A., Rush, J., Morrice, N., and Kirschner, M. W. (2006) Phosphorylation analysis by mass spectrometry: myths, facts, and the consequences for qualitative and quantitative measurements. *Mol. Cell. Proteomics* **5,** 172–181
22. Ficarro, S. B., McCleland, M. L., Stukenberg, P. T., Burke, D. J., Ross, M. M., Shabanowitz, J., Hunt, D. F., and White, F. M. (2002) Phosphoproteome analysis by mass spectrometry and its application to Saccharomyces cerevisiae. *Nat. Biotechnol.* **20,** 301–305
23. Pinkse, M. W., Uitto, P. M., Hilhorst, M. J., Ooms, B., and Heck, A. J. (2004) Selective isolation at the femtomole level of phosphopeptides from proteolytic digests using 2D-NanoLC-ESI-MS/MS and titanium oxide precolumns. *Anal. Chem.* **76,** 3935–3943
24. Ballif, B. A., Roux, P. P., Gerber, S. A., MacKeigan, J. P., Blenis, J., and Gygi, S. P. (2005) Quantitative phosphorylation profiling of the ERK/p90 ribosomal S6 kinase-signaling cassette and its targets, the tuberous sclerosis tumor suppressors. *Proc. Natl. Acad. Sci. U. S. A.* **102,** 667–672
25. Blagoev, B., Ong, S. E., Kratchmarova, I., and Mann, M. (2004) Temporal analysis of phosphotyrosine-dependent signaling networks by quantitative proteomics. *Nat. Biotechnol.* **22,** 1139–1145
26. Gruhler, A., Olsen, J. V., Mohammed, S., Mortensen, P., Faergeman, N. J., Mann, M., and Jensen, O. N. (2005) Quantitative phosphoproteomics applied to the yeast pheromone signaling pathway. *Mol. Cell. Proteomics* **4,** 310–327
27. Kim, J. E., and White, F. M. (2006) Quantitative analysis of phosphotyrosine signaling networks triggered by CD3 and CD28 costimulation in Jurkat cells. *J. Immunol*. **176,** 2833–2843
28. Sachon, E., Mohammed, S., Bache, N., and Jensen, O. N. (2006) Phosphopeptide quantitation using amine-reactive isobaric tagging reagents and tandem mass spectrometry: application to proteins isolated by gel electrophoresis. *Rapid Commun. Mass Spectrom.* **20,** 1127–1134
29. Axelos, M., Curie, C., Mazzolini, L., Bardet, C., and Lescure, B. (1992) A protocol for transient gene expression in Arabidopsis thaliana protoplasts isolated from cell suspension cultures. *Plant Physiol. Biochem.* **30,** 123–128
30. Larsson, C., Sommarin, M., and Widell, S. (1994) Isolation of highly purified plant plasma membranes and separation of inside-out and right-side-out vesicles. *Methods Enzymol.* **228,** 451–469
31. Gobom, J., Nordhoff, E., Mirgorodskaya, E., Ekman, R., and Roepstorff, P. (1999) Sample purification and preparation technique based on nanoscale reversed-phase columns for the sensitive analysis of complex peptide mixtures by matrix-assisted laser desorption/ionization mass spectrometry. *J. Mass Spectrom.* **34,** 105–116
32. Alexandersson, E., Saalbach, G., Larsson, C., and Kjellbom, P. (2004) Arabidopsis plasma membrane proteomics identifies components of transport, signal transduction and membrane trafficking. *Plant Cell Physiol.* **45,** 1543–1556
33. Marmagne, A., Rouet, M. A., Ferro, M., Rolland, N., Alcon, C., Joyard, J., Garin, J., Barbier-Brygoo, H., and Ephritikhine, G. (2004) Identification of new intrinsic proteins in Arabidopsis plasma membrane proteome. *Mol. Cell. Proteomics* **3,** 675–691
34. Nuhse, T. S., Stensballe, A., Jensen, O. N., and Peck, S. C. (2003) Large-scale analysis of in vivo phosphorylated membrane proteins by immobilized metal ion affinity chromatography and mass spectrometry. *Mol. Cell. Proteomics* **2,** 1234–1243
35. Beausoleil, S. A., Jedrychowski, M., Schwartz, D., Elias, J. E., Villen, J., Li, J., Cohn, M. A., Cantley, L. C., and Gygi, S. P. (2004) Large-scale characterization of HeLa cell nuclear phosphoproteins. *Proc. Natl. Acad. Sci. U. S. A.* **101,** 12130–12135
36. Larsen, M. R., Thingholm, T. E., Jensen, O. N., Roepstorff, P., and Jorgensen, T. J. (2005) Highly selective enrichment of phosphorylated peptides from peptide mixtures using titanium dioxide microcolumns. *Mol. Cell. Proteomics* **4,** 873–886
37. Oda, Y., Huang, K., Cross, F. R., Cowburn, D., and Chait, B. T. (1999) Accurate quantitation of protein expression and site-specific phosphorylation. *Proc. Natl. Acad. Sci. U. S. A.* **96,** 6591–6596
38. Ong, S. E., Blagoev, B., Kratchmarova, I., Kristensen, D. B., Steen, H., Pandey, A., and Mann, M. (2002) Stable isotope labeling by amino acids in cell culture, SILAC, as a simple and accurate approach to expression proteomics. *Mol. Cell. Proteomics* **1,** 376–386
39. Gruhler, A., Schulze, W. X., Matthiesen, R., Mann, M., and Jensen, O. N. (2005) Stable isotope labeling of Arabidopsis thaliana cells and quantitative proteomics by mass spectrometry. *Mol. Cell. Proteomics* **4,** 1697–1709
40. Krijgsveld, J., Ketting, R. F., Mahmoudi, T., Johansen, J., Artal-Sanz, M., Verrijzer, C. P., Plasterk, R. H., and Heck, A. J. (2003) Metabolic labeling of C. elegans and D. melanogaster for quantitative proteomics. *Nat. Biotechnol.* **21,** 927–931
41. Dunkley, T. P., Hester, S., Shadforth, I. P., Runions, J., Weimar, T., Hanton, S. L., Griffin, J. L., Bessant, C., Brandizzi, F., Hawes, C., Watson, R. B., Dupree, P., and Lilley, K. S. (2006) Mapping the Arabidopsis organelle proteome. *Proc. Natl. Acad. Sci. U. S. A.* **103,** 6518–6523
42. Bargmann, B. O., Laxalt, A. M., Riet, B. T., Schouten, E., van Leeuwen, W., Dekker, H. L., de Koster, C. G., Haring, M. A., and Munnik, T. (2006) LePLDβ1 activation and relocalization in suspension-cultured tomato cells treated with xylanase. *Plant J.* **45,** 358–368
43. Xing, T., Higgins, V. J., and Blumwald, E. (1997) Race-specific elicitors of Cladosporium fulvum promote translocation of cytosolic components of NADPH oxidase to the plasma membrane of tomato cells. *Plant Cell* **9,** 249–259
44. Veronese, P., Nakagami, H., Bluhm, B., Abuqamar, S., Chen, X., Salmeron, J., Dietrich, R. A., Hirt, H., and Mengiste, T. (2006) The membrane-anchored BOTRYTIS-INDUCED KINASE1 plays distinct roles in Arabidopsis resistance to necrotrophic and biotrophic pathogens. *Plant Cell* **18,** 257–273
45. Allwood, E. G., Davies, D. R., Gerrish, C., and Bolwell, G. P. (2002) Regulation of CDPKs, including identification of PAL kinase, in biotically stressed cells of French bean. *Plant Mol. Biol.* **49,** 533–544
46. Romeis, T., Ludwig, A. A., Martin, R., and Jones, J. D. (2001) Calcium-dependent protein kinases play an essential role in a plant defence response. *EMBO J.* **20,** 5556–5567
47. Robatzek, S., Chinchilla, D., and Boller, T. (2006) Ligand-induced endocytosis of the pattern recognition receptor FLS2 in Arabidopsis. *Genes Dev.* **20,** 537–542
48. Conrath, U., Pieterse, C. M., and Mauch-Mani, B. (2002) Priming in plant-pathogen interactions. *Trends Plant Sci.* **7,** 210–216
49. Verhagen, B. W., Glazebrook, J., Zhu, T., Chang, H. S., van Loon, L. C., and Pieterse, C. M. (2004) The transcriptome of rhizobacteria-induced systemic resistance in Arabidopsis. *Mol. Plant-Microbe Interact.* **17,** 895–908
50. van Loon, L. C., Bakker, P. A., and Pieterse, C. M. (1998) Systemic resistance induced by rhizosphere bacteria. *Annu. Rev. Phytopathol.* **36,** 453–483
51. Navarro, L., Dunoyer, P., Jay, F., Arnold, B., Dharmasiri, N., Estelle, M., Voinnet, O., and Jones, J. D. (2006) A plant miRNA contributes to antibacterial resistance by repressing auxin signaling. *Science* **312,** 436–439
52. Kovtun, Y., Chiu, W. L., Zeng, W., and Sheen, J. (1998) Suppression of auxin signal transduction by a MAPK cascade in higher plants. *Nature* **395,** 716–720
53. Liu, Y., and Zhang, S. (2004) Phosphorylation of 1-aminocyclopropane-1-carboxylic acid synthase by MPK6, a stress-responsive mitogen-activated protein kinase, induces ethylene biosynthesis in Arabidopsis. *Plant Cell* **16,** 3386–3399
54. Pearson, G., Robinson, F., Beers Gibson, T., Xu, B.-e., Karandikar, M., Berman, K., and Cobb, M. H. (2001) Mitogen-activated protein (MAP) kinase pathways: regulation and physiological functions. *Endocr. Rev.* **22,** 153–183
55. Cano-Delgado, A., Penfield, S., Smith, C., Catley, M., and Bevan, M. (2003) Reduced cellulose synthesis invokes lignification and defense responses in Arabidopsis thaliana. *Plant J.* **34,** 351–362
56. Ellis, C., Karafyllidis, I., Wasternack, C., and Turner, J. G. (2002) The

Arabidopsis mutant cev1 links cell wall signaling to jasmonate and ethylene responses. *Plant Cell* **14,** 1557–1566
57. Collins, N. C., Thordal-Christensen, H., Lipka, V., Bau, S., Kombrink, E., Qiu, J. L., Huckelhoven, R., Stein, M., Freialdenhoven, A., Somerville, S. C., and Schulze-Lefert, P. (2003) SNARE-protein-mediated disease resistance at the plant cell wall. *Nature* **425,** 973–977
58. Stein, M., Dittgen, J., Sanchez-Rodriguez, C., Hou, B. H., Molina, A., Schulze-Lefert, P., Lipka, V., and Somerville, S. (2006) Arabidopsis PEN3/PDR8, an ATP binding cassette transporter, contributes to nonhost resistance to inappropriate pathogens that enter by direct penetration. *Plant Cell* **18,** 731–746
59. Torres, M. A., and Dangl, J. L. (2005) Functions of the respiratory burst oxidase in biotic interactions, abiotic stress and development. *Curr. Opin. Plant Biol.* **8,** 397–403
60. Davies, D. R., Bindschedler, L. V., Strickland, T. S., and Bolwell, G. P. (2006) Production of reactive oxygen species in Arabidopsis thaliana cell suspension cultures in response to an elicitor from Fusarium oxysporum: implications for basal resistance. *J. Exp. Bot.* **57,** 1817–1827
61. Levine, A., Tenhaken, R., Dixon, R., and Lamb, C. (1994) H_2O_2 from the oxidative burst orchestrates the plant hypersensitive disease resistance response. *Cell* **79,** 583–593
62. Torres, M. A., Dangl, J. L., and Jones, J. D. (2002) Arabidopsis gp91phox homologues AtrbohD and AtrbohF are required for accumulation of reactive oxygen intermediates in the plant defense response. *Proc. Natl. Acad. Sci. U. S. A.* **99,** 517–522
63. Lipka, V., Dittgen, J., Bednarek, P., Bhat, R., Wiermer, M., Stein, M., Landtag, J., Brandt, W., Rosahl, S., Scheel, D., Llorente, F., Molina, A., Parker, J., Somerville, S., and Schulze-Lefert, P. (2005) Pre- and post-invasion defenses both contribute to nonhost resistance in Arabidopsis. *Science* **310,** 1180–1183
64. Nuhse, T. S., Boller, T., and Peck, S. C. (2003) A plasma membrane syntaxin is phosphorylated in response to the bacterial elicitor flagellin. *J. Biol. Chem.* **278,** 45248–45254
65. Assaad, F. F., Qiu, J. L., Youngs, H., Ehrhardt, D., Zimmerli, L., Kalde, M., Wanner, G., Peck, S. C., Edwards, H., Ramonell, K., Somerville, C. R., and Thordal-Christensen, H. (2004) The PEN1 syntaxin defines a novel cellular compartment upon fungal attack and is required for the timely assembly of papillae. *Mol. Biol. Cell* **15,** 5118–5129
66. Bhat, R. A., Miklis, M., Schmelzer, E., Schulze-Lefert, P., and Panstruga, R. (2005) Recruitment and interaction dynamics of plant penetration resistance components in a plasma membrane microdomain. *Proc. Natl. Acad. Sci. U. S. A.* **102,** 3135–3140
67. McDonald, H. B., Stewart, R. J., and Goldstein, L. S. (1990) The kinesin-like ncd protein of Drosophila is a minus end-directed microtubule motor. *Cell* **63,** 1159–1165
68. Praefcke, G. J., and McMahon, H. T. (2004) The dynamin superfamily: universal membrane tubulation and fission molecules? *Nat. Rev. Mol. Cell. Biol.* **5,** 133–147
69. Roepstorff, P., and Fohlman, J. (1984) Proposal for a common nomenclature for sequence ions in mass spectra of peptides. *Biomed. Mass Spectrom.* **11,** 601
70. Schulze, W. X., and Mann, M. (2004) A novel proteomic screen for peptide-protein interactions. *J. Biol. Chem.* **279,** 10756–10764